Proceedings of Modeling of Casting and Solidification Processes VI, 2004
Edited by HWANG Weng-Sing

GLOBULAR EQUIAXED SOLIDIFICATION WITH THERMO-SOLUTAL CONVECTION, SHRINKAGE FLOW AND GRAIN MOVEMENT BY A THREE-PHASE MODEL

Tongmin Wang[1], Menghuai Wu[2], Andreas Ludwig[2], Merly Abondano[1], Björn Pustal[1], Andreas Bührig-Polaczek[1]

1 Foundry Institute, Aachen University of Technology; Intzestr.5; Aachen, D-52072, Germany
2 Department of Metallurgy, University of Leoben; Franz-Josef-Str.18; Leoben, A-8700, Austria

Keywords: Three-phase, Free surface, Thermo-solutal convection, Shrinkage flow, Grain movement

Abstract

A Three-Phase Model is developed to simulate the globular equiaxed solidification. The three phases are liquid, solid and air, respectively. We solved the basic conservation equations of mass, momentum, enthalpy for each phase, and considered the thermal and mechanical (drag force) interactions among the phases. Grain nucleation, growth rate (mass exchange), solute partitioning at liquid-solid interface and solute transport are also accounted for. Due to its small density, the air phase floats always at the top region, forming a definable air-liquid melt interface, i.e. free surface. By tracking this free surface, the shrinkage cavity in an open casting system can be modeled. As the temperature and concentration dependent density and solidification shrinkage are explicitly included, the thermo-solutal convection, together with feeding flow and grain movement can be taken into account. This paper focuses on the model description, and the preliminary results on a benchmark ingot casting (Al-4wt%Cu) are presented and discussed.

1. Introduction

Melt convection and grain movement play an important role in casting solidification process, which greatly influence the formation of grain structures and solute segregations. In general, the melt convection and grain movement are a result of gravitational force. The densities within melt are different due to the variation of temperature and concentration, and the density differences under gravitational field cause the melt convection as called thermo-solutal convection. As the same, the density differences between the grains and the bulk melt cause the grain movement as called solid sedimentation or grain floating. Additionally, another driving force for melt convection and grain movement is the solidification shrinkage. It is well known that solidification shrinkage is the main reason of forming shrinkage cavity and one of the dominate reasons of causing porosity, hot/cold-tearing, stress and deformation etc. Shrinkage force could somehow affect the flow pattern and the macrosegregation formation. This is early described by J. Campbell in his book for explaining the macrosegregation formation in a steel ingot casting [1]. The vast majority of casting solidification models neglect the shrinkage-induced flow (feeding flow) for simplification. The thermo-solutal convection modeling without consideration of shrinkage effect is generally realized by employing the well-known Boussinesq approximation [2]. As well, the assumption of ignoring shrinkage effect in our previous work is declared [3-5]. To further consider shrinkage flow, the modeling of free surface is necessary because the shape of free surface and the physical values near free surface dynamically changes during solidification.

In this paper, we track the moving free surface due to solidification shrinkage by a three-phase approach as well model the melt density as temperature and concentration dependent, so that both

the shrinkage flow and thermo-solutal convection can be taken into account. Special care is taken on the change of heat, momentum and pressure near the free surface. Meanwhile, the model considers nucleation and growth of globular equiaxed grain growth, solute transport by diffusion and convection. The following points are finally discussed based on the calculations by applying the present model to a benchmark casting: the shape of free surface and the pressure change near free surface with/without consideration of grain movement, the flow pattern and macrosegregation formation with/without consideration of shrinkage flow.

2. Model Description

There are totally three phases involved in the globular equiaxed solidification process: the liquid melt, the solidifying grains and the sucked air, denoted by l, s, a respectively. We employ a volume averaging approach to formulate the conservation equations of mass, momentum, species, and enthalpy for the three phases.

2.1 Conservation Equations

Mass:

$$\frac{\partial}{\partial t}(f_l \rho_l) + \nabla \cdot (f_l \rho_l \mathbf{u}_l) = M_{sl} \tag{1}$$

$$\frac{\partial}{\partial t}(f_s \rho_s) + \nabla \cdot (f_s \rho_s \mathbf{u}_s) = M_{ls} \tag{2}$$

$$\frac{\partial}{\partial t}(f_a \rho_a) + \nabla \cdot (f_a \rho_a \mathbf{u}_a) = 0 \tag{3}$$

$$f_l + f_s + f_a = 1 \tag{4}$$

Note that the air has no mass transfer with other phases, therefore the source term of Eq.(3) is zero.

Momentum:

$$\frac{\partial}{\partial t}(f_l \rho_l \mathbf{u}_l) + \nabla \cdot (f_l \rho_l \mathbf{u}_l \otimes \mathbf{u}_l) = -f_l \nabla p + \nabla \cdot \overline{\overline{\tau}}_l + f_l \rho_l \mathbf{g} + \mathbf{U}_{sl} + \mathbf{U}_{al} \tag{5}$$

$$\frac{\partial}{\partial t}(f_s \rho_s \mathbf{u}_s) + \nabla \cdot (f_s \rho_s \mathbf{u}_s \otimes \mathbf{u}_s) = -f_s \nabla p + \nabla \cdot \overline{\overline{\tau}}_s + f_s \rho_s \mathbf{g} + \mathbf{U}_{ls} + \mathbf{U}_{as} \tag{6}$$

$$\frac{\partial}{\partial t}(f_a \rho_a \mathbf{u}_a) + \nabla \cdot (f_a \rho_a \mathbf{u}_a \otimes \mathbf{u}_a) = -f_a \nabla p + \nabla \cdot \overline{\overline{\tau}}_a + f_a \rho_a \mathbf{g} + \mathbf{U}_{la} + \mathbf{U}_{sa} \tag{7}$$

where $\overline{\overline{\tau}}_l = \mu_l f_l \cdot \left(\nabla \otimes \mathbf{u}_l + (\nabla \otimes \mathbf{u}_l)^T\right)$ $\quad$ $\overline{\overline{\tau}}_s = \mu_s f_s \cdot \left(\nabla \otimes \mathbf{u}_s + (\nabla \otimes \mathbf{u}_s)^T\right)$

$\overline{\overline{\tau}}_a = \mu_a f_a \cdot \left(\nabla \otimes \mathbf{u}_a + (\nabla \otimes \mathbf{u}_a)^T\right)$

Species:

$$\frac{\partial}{\partial t}(f_l \rho_l \mathbf{u}_l) + \nabla \cdot (f_l \rho_l \mathbf{u}_l c_l) = \nabla \cdot (f_l \rho_l D_l \nabla c_l) + C_{sl} \tag{8}$$

$$\frac{\partial}{\partial t}(f_s \rho_s \mathbf{u}_s) + \nabla \cdot (f_s \rho_s \mathbf{u}_s c_s) = \nabla \cdot (f_s \rho_s D_s \nabla c_s) + C_{ls} \tag{9}$$

Note that the species calculation has been omitted for the air phase since there is no species mass fraction within the air phase.

Enthalpy:

$$\frac{\partial}{\partial t}(f_l \rho_l h_l) + \nabla \cdot (f_l \rho_l \mathbf{u}_l h_l) = \nabla \cdot (f_l k_l \nabla \cdot T_l) + Q_{sl} + Q_{al} \tag{10}$$

$$\frac{\partial}{\partial t}(f_s \rho_s h_s) + \nabla \cdot (f_s \rho_s \mathbf{u}_s h_s) = \nabla \cdot (f_s k_s \nabla \cdot T_s) + Q_{ls} + Q_{as} \tag{11}$$

$$\frac{\partial}{\partial t}(f_a \rho_a h_a) + \nabla \cdot (f_a \rho_a \mathbf{u}_a h_a) = \nabla \cdot (f_a k_a \nabla \cdot T_a) + Q_{la} + Q_{sa} \tag{12}$$

where $h_l = \int_{Tref}^{T_l} c_{p(l)} dT + h_l^{ref}$ $\quad h_s = \int_{Tref}^{T_s} c_{p(s)} dT + h_s^{ref}$ $\quad h_a = \int_{Tref}^{T_a} c_{p(a)} dT + h_a^{ref}$

Grain Transport:

$$\frac{\partial}{\partial t} n + \nabla \cdot (\mathbf{u}_s \cdot n) = N \tag{13}$$

where f is the volume fraction, $\mathbf{u}$ is the velocity vector, c is the mass fraction of species, h is the enthalpy and T the temperature, n is the grain density, $\mathbf{g}$ is the gravity vector, p is the pressure, τ is strain tensor, μ is viscosity, ρ is the density, k is the thermal conductivity, c_p is specific heat, M is a source term representing the mass transfer between liquid and solid, N is a source term representing the grain nucleation rate, $\mathbf{U}, C, Q$ are the source terms caused by a mechanical or thermal interaction and a phase change, subscript l, s, a denote the liquid, solid and air phases respectively and their combinations denote the corresponding group of phases. All the physical parameters appearing in the conservation equations above follow the concept of "volume average". The corresponding source terms $\mathbf{U}_{xx}, M_{xx}, C_{xx}, Q_{xx}, N$ will be described in the following sections. Please refer to our previous work [3-6] for more details of the descriptions of the nucleation, growth kinetics and mass transfer rate definition, solute partitioning at liquid-solid interface, enthalpy transfer between liquid and solid phases. The differences here are the case of air phase presence is modeled, that is, the shrinkage flow effect is further considered.

2.2 Momentum Transfer

Phase interactions (e.g. drag and friction) denoted by superscript d and phase change denoted by superscript p are considered to calculate the momentum source terms. Therefore for a liquid-solid mixture, we have

$$\mathbf{U}_{ls} = -\mathbf{U}_{sl} = \mathbf{U}_{ls}^{p} + \mathbf{U}_{ls}^{d} \tag{14}$$

with $\mathbf{U}_{ls}^{p} = \mathbf{u}^{*} \cdot M_{ls}$ and $\mathbf{U}_{ls}^{d} = K_{ls}\left(\mathbf{u}_l - \mathbf{u}_s\right)$.

We have $u^{*} = u_l$ for solidification and $u^{*} = u_s$ for remelting. The drag force coefficient, K_{ls}, is calculated by employing the model developed by Wang et al [7].

$$K_{ls} = \frac{4\beta^2 \mu_l}{d_s^{\,2}} f_l^2 \tag{15}$$

$$\beta = \left[\frac{9}{2}(1-f_l) \frac{2+\frac{4}{3}\eta^5}{2-3\eta+3\eta^5-2\eta^6} \frac{1}{C_p(\phi_e)} \right]^{1/2}$$

with

$$\eta = (1-f_l)^{1/3}$$

$$C_p(\phi_e) = \phi_e^2 \qquad 0.0 < f_l < 0.7$$

$$C_p(\phi_e) = 1.26 \log_{10}\left(\frac{\phi_e}{0.163}\right) \qquad 0.7 < f_l < 1.0$$

where d_s is the grain diameter, $C_p(\phi_e)$ is a correction factor accounts for the shape of dendrite envelope. The above calculation of drag force coefficient is a rather universal method and adapt for globular, equiaxed and columnar growth. ϕ_e can be simplified as 1 in case of globular growth.

The momentum source terms due to phase change between air and solid or liquid are neglected. Therefore, for liquid-air and solid-air mixtures, the source terms are calculated by

$$\mathbf{U}_{la} = -\mathbf{U}_{al} = \mathbf{U}_{la}^d = K_{la}\left(\mathbf{u}_l - \mathbf{u}_a\right) \tag{16}$$

$$\mathbf{U}_{sa} = -\mathbf{U}_{as} = \mathbf{U}_{sa}^d = K_{sa}\left(\mathbf{u}_s - \mathbf{u}_a\right) \tag{17}$$

Schiller and Naumann`s model is used for calculating K_{la} [8].

$$K_{la} = 3\mu_l f_l f_a C_D R_e / (4 d_a^2) \tag{18}$$

where d_a is the characteristic diameter of air, C_D is drag coefficient that is based on the relative Reynolds number R_e.

$$C_D = \begin{cases} 24(1+0.15R_e^{0.687})/R_e & R_e \le 1000 \\ 0.44 & R_e > 1000 \end{cases} \tag{19}$$

with $R_e = \dfrac{\rho_l |\mathbf{u}_a - \mathbf{u}_l| d_a}{\mu_l}$

Symmetric model is used for calculating K_{sa}. Symmetric model is similar with Schiller and Naumann`s model. The difference is that, the average grain diameter of air and solid $(d_a + d_s)/2$, the mixed viscosity $\mu_a f_a + \mu_s f_s$ and the mixed density $\rho_a f_a + \rho_s f_s$ are used in the calculation instead of using the properties of a single phase only.

2.3 Enthalpy Transfer

The source terms of enthalpy transfer for liquid/air and solid/air mixtures are calculated by

$$Q_{la} = Q_{la}^d = H_{la} \cdot \left(T_l - T_a\right) \tag{20}$$

$$Q_{sa} = Q_{sa}^d = H_{sa} \cdot \left(T_s - T_a\right) \tag{21}$$

Note that the parts due to phase change are also neglected. The heat exchange coefficient, H_{la} is calculated by the Ranz and Marshall model [8]

$$H_{la} = 6\lambda_l f_l f_s Nu_p / d_a^2 \tag{22}$$

$$H_{sa} = h_{sa} f_s f_a \tag{23}$$

where Nu_p is the Nusselt number, h_{sa} is an empirical heat transfer coefficient independent of mass fraction.

2.4 Thermo-solutal Convection and Shrinkage Flow

The temperature and concentration dependence of the melt density is given by [2]:

$$\rho_l = \rho_l(T, c_l) = \rho_0(1 - \beta_T(T - T_0) - \beta_c(c_l - c_0)) \tag{24}$$

where ρ_0 is a reference density of liquid phase taken at temperature T_0 and species mass fraction c_0, and β_T, β_c are the thermal and solutal expansion coefficients, respectively. The solid density ρ_s is assumed to be a constant. The density defined by Eq.(24) will reflect the shrinkage flow and thermo-solutal convection when it appears in the mass and momentum conservation equations of the three-phase model. However the conventional Bousinesq approximation considers the Eq.(24) for the Momentum equation only with ignoring the effects of solidification shrinkage. It is realized by adding the additional gravity terms (buoyancy force) to the momentum equations [2].

The conservation equations (Eqs. (1)-(13)) are numerically solved by using a fully implicit and control-volume-based finite difference method. A CFD software FLUENT (Ver. 6.1) is used here.

Table-I Thermophysical and thermodynamic Properties used in the simulation [6, 9]

ρ_l	$\rho_l = \rho_0(1 - \beta_T(T - T_0) - \beta_c(c_l - c_0))$ $\rho_0 = 2606 \quad kg/m^3$ $\beta_T = 1\times10^{-4} \quad 1/K$ $\beta_c = -9.2\times10^{-3} \quad 1/wt\%$
ρ_s, ρ_a	$2743, 1.225\, kg/m^3$
k_l, k_s, k_a	77, 153, 0.0242 W/m/K
$c_{p(l)}, c_{p(s)}, c_{p(a)}$	1179, 766, 1006.43 J/Kg/K
D_l, D_s	5×10^{-9} , 5×10^{-13} m^2/s
μ_l, μ_a	1.2×10^{-3} , 1.8×10^{-5} $kg/m/s$
$\mu_s = \begin{cases} \frac{\mu_l}{f_s}\cdot\left(\left(1-f_s/f_s^c\right)^{-2.5 f_s^c} - \left(1-f_s\right)\right) & when \ f_s < f_s^c \\ \infty & else \end{cases}$ with the packing limit $f_s^c = 0.637$	
T_f	933.5 K
k	0.145
m	-344 K

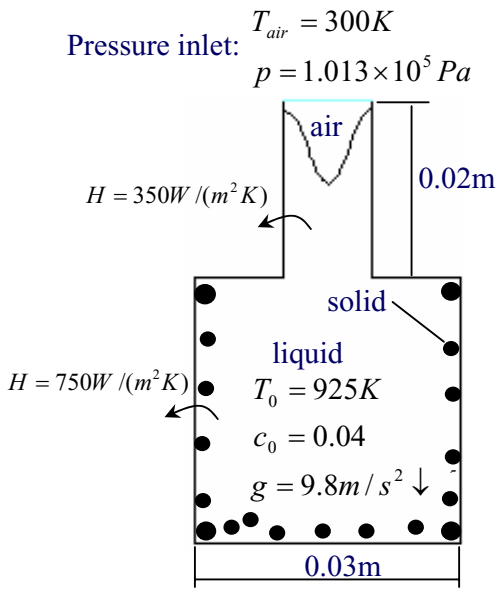

Fig.1 A benchmark of ingot casting (Al-4wt%Cu) and the schematic diagram of three phases

3. Results and Discussion

In order to study the free surface formation and the impact of shrinkage flow on the flow pattern and macrosegregation, we consider an ingot casting benchmark with small geometry as shown in Fig.1. The melt is supposed to be filled instantaneously. We selected an inoculated Al-4wt%Cu alloy because of its almost globular equiaxed solidification morphology. Table-I shows the physical properties of this alloy and of air.

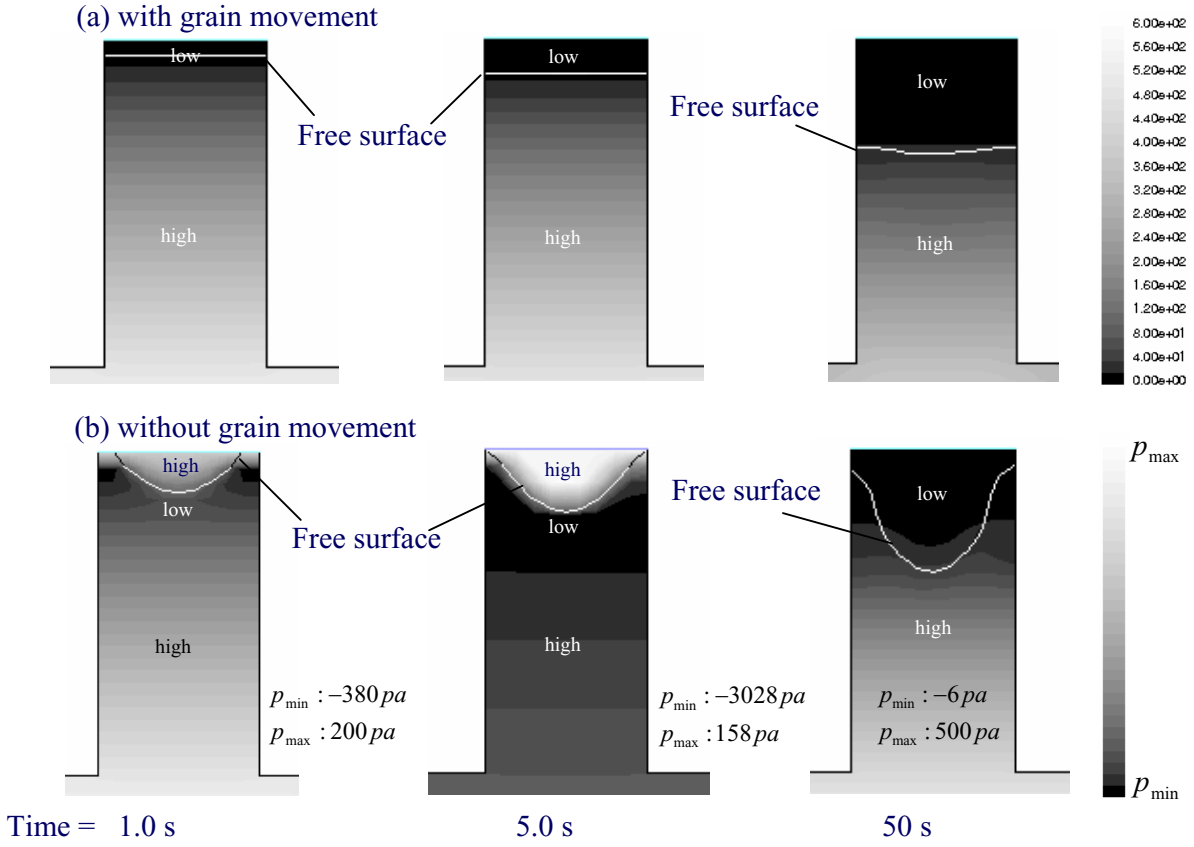

Fig.2 The free surface (line) and the total pressure distribution (gray scale) near the free surface

Fig. 2 shows the free surface and the total pressure distribution near the free surface with and without grain movement. The free surface is defined as the isoline of air phase fraction = 50%. It is noted that both the shape of free surface and the distribution of total pressure look rather straight in case of grain movement (see Fig.2 (a)). The total pressure increases towards to the bottom mainly due to the metallostatic pressure. A quite low pressure occurs at the top area because the density of sucked air is rather small thus a minor hydrostatic pressure. Note that the standard 1 bar ambient pressure is excluded here since it equally appears everywhere of the melt. The melt flow does not meet any hindering force while feeding the shrinking cavity since the grains near the free surface can freely move following the feeding melt. Although the packing limit of solid fraction is set to 0.637, the assuming cooling conditions make the heat transfer bigger in the mold part and lower in the riser-like part. It ensures the solidification occurs firstly in the mold part and then the riser-like part. Only at the end of solidification (time = 50 s), the solidification fraction finally reaches the packing limit, then the grain movement is constrained according to the packing limit assumption. Therefore, we can see that the shape of free surface changes a little its curvature due to the

hindering of the constrainable grains. In case of no grain movement (see Fig. 2(b)), both the shape of free surface and the distribution of total pressure are quite different as compared with those of Fig. 2(a). The shape of free surface tends to be curvatured. The pressure above the free surface rises intensely. There forms an obvious negative pressure area below the free surface. The melt is driven by the shrinkage force to feed the shrinking cavity but hindered by the no-move grains. A large pressure gradient is formed around the free surface due to the difference of forces. After the metallostatic pressure is also included, the distribution of total pressure finally looks like a high-low-high landscape (see Fig.2(b) with time = 1.0s, 5.0s). At the end of solidification (time = 50s), the high pressure above the free surface disappears because the shrinkage-induced pressure gradient is gone after the feeding flow path is closed. In fact, the cases of Fig.2 (a) and (b) are the extreme cases. The reality of grain movement is neither a completely free one nor a constraining one. Therefore the shape of free surface and the distribution of total pressure in the reality should be a case between Fig.2 (a) and (b).

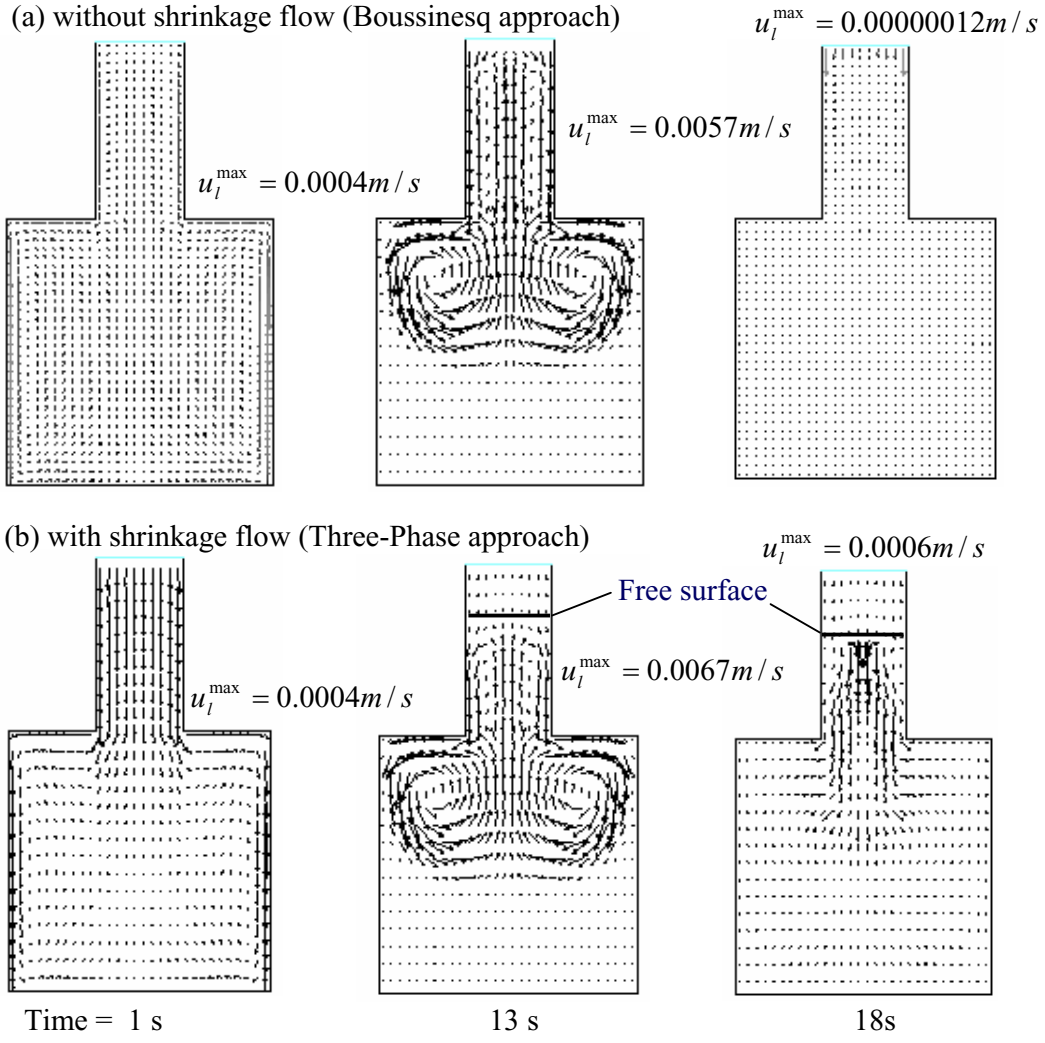

Fig.3 The melt flow patterns consisting of thermo-solutal convection, grain movement and with/without shrinkage flow

Fig.3 shows the flow pattern variation of the solidifying sample in case of absence and presence of shrinkage flow. At the very beginning (time = 1 s), it is noted that there are strong flows near the mold walls for the cases of both Fig.3 (a) and (b). It is due to a fast melt cooling near the mold walls

increasing the density there and activating the thermal convection. The solutal convection is minor because the solute has not piled up yet. Particularly the shrinkage flow from top to feed the shrinking melt is obviously observed in Fig.3 (b). The shrinkage flow and thermal convection dominate the flow pattern at the beginning according to the findings above. While solidification proceeds, the flow is becoming a combination of thermo-solutal convection and shrinkage flow. Because of the solute partition and transport and the further melt cooling and heat transfer, the thermo-solutal convection dominates the flow pattern and the shrinkage flow is hardly watched, although it exists (see Fig.3 (a) and (b) with time = 13 s). There is minor velocity at the top of riser-like part in Fig.3 (b) due to the occupation of sucked air. With the further solidification, the space available for the melt convection is becoming smaller and smaller. Therefore, the thermo-solutal convection is becoming weaker and weaker (see Fig.3 (a) with time = 18 s). However, the shrinkage flow is still active because our assuming cooling condition ensures the feeding path unblocked till to the solidification end (see Fig.3 (b) with time = 18 s). It can be concluded that the shrinkage flow dominates the flow pattern in this situation.

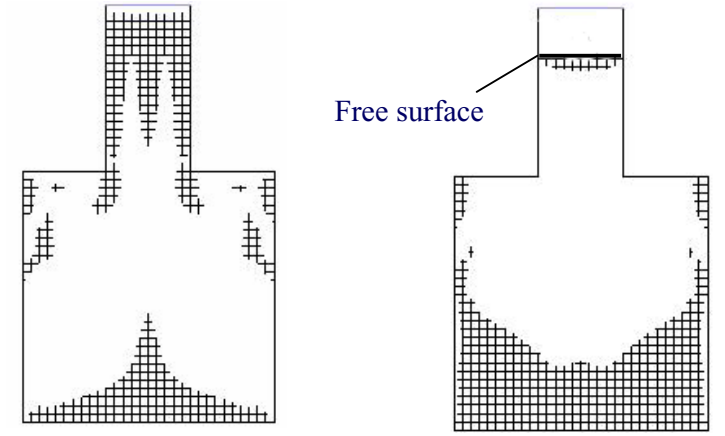

(a) without shrinkage flow (b) with shrinkage flow

Fig.4 The positive macro-segregation maps near the solidification end by considering thermo-solutal convection, grain movement, and with/without shrinkage flow (c_{mix} : 4.1 wt% - 4.3 wt%)

Fig.4 shows the positive macrosegregation maps near the solidification end in case of absence and presence of shrinkage flow. The absolute values of positive segregation in the cases of Fig.4 (a) and (b) are not big (c_{mix} : 4.1wt%-4.3wt% as compared with the initial concentration 4wt%) because the benchmark used for simulation is rather small thus a short solidification time. However we still notice the big differences of segregation maps comparing the predictions with and without consideration of the shrinkage flow. Two obvious differences: 1) the positive segregation area without consideration of shrinkage flow is bigger than that with consideration of shrinkage flow at the top of riser-like part; 2) the positive segregation map looks like a tower without consideration of shrinkage flow and the one with consideration shrinkage flow looks like a bowl at the bottom of the casting. The more results and detailed analysis will be presented in the following papers.

4. Concluding Remarks

The developed three-phase model is applied to simulate a benchmark ingot casting. The results show that the presented model is feasible to model the thermo-solutal convection together with

grain movement and shrinkage flow for a globular exquiaxed solidification. The following remarks could be concluded from the testing calculation.

1) The shape of free surface and the distribution of total pressure near the free surface are almost straight in case of free grain movement, and largely curvatured in case of grain-no-movement. It was found that the pressure intensely rises above the free surface in case of grain-no-movement.
2) For the benchmark casting, the comprehensive flow pattern consisting of thermo-solutal convection and shrinkage flow is firstly dominated by the thermal convection and shrinkage flow, then by the thermo-solutal convection and finally by the shrinkage flow during solidification.
3) The absolute macrosegregation are not serious, but a very big difference of positive segregation patterns is found if we compare the cases with and without considering shrinkage flow.

Acknowledgements

Financial support for this research has been provided by the German Science Foundation (DFG) as part of the collaborative research center SFB 370.

References

1. J. Campbell, Castings, (Oxford: Butterworth-Heinemann Ltd, 1991)

2. Th. U. Kaempfer, M. Rappaz, “Numerical modelling of macrosegregation during solidification processes using multiple, adaptive finite element grids”, (paper presented at the Modeling of Casting, Welding and Advanced Solidification Processes IX, Aachen, Germany, 20, August 2000), 640-645.

3. M. Wu, A. Ludwig, “Influence of Phase-Transport Phenomena on Macrosegregation and Strucutre Formation During Solidification” *Adv. Eng. Mater.,* vol. 5, No. 1-2, 2003, 62-66.

4. M. Wu, A. Ludwig, A. Bührig-Polaczek, M. Fehlbier, P.R. Sahm, “Influence of convection and grain movement on globular equiaxed solidification,” Int. *J. Heat Mass Transfer*., Vol 46, 2003, 2819-2832.

5. A. Ludwig, M. Wu, T. Wang and A. Bührig-Polaczek, “About the interaction between thermo-solutal convection and grain sedimentation during globular equiaxed solidification,” (paper submitted for the the 3rd Int. Conf. on Comp. Model. Sim. Mater, Italy, 2004)

6. A. Ludwig, M. Wu, “Modeling of Globular Equiaxed Solidification with a Two-Phase Approach,” *Metall. Mater. Trans*. Vol. 33A , 2002, 3673.

7. C.Y. Wang, S. Ahuja, C. Beckermann, and H.C. de Groh III, “Multiparticle Interfacial Drag in Equiaxed Solidification,“ *Metall. Mater. Trans.* vol. 26B, No.2, 1995, 111-119

8. FLUENT 4.4 User`s Guide Volume 2, chapter 9, 16-29

9. R. Trivedi, S. Liu, P. Mazumder, E. Simsek, *Sci. Techn. Adv. Mater*., Vol 2, 2001, 309-320.